International Journal of Engineering and Advanced Technology (IJEAT)
ISSN: 2249-8958 (Online), Volume-8 Issue-5, June 2019

Intensity Index Based Histogram Equalization Technique for retinal Image Enhancement and Classification of Hard Exudates using Supervised Learning

Arun Pradeep, X. Felix Joseph

Abstract*: *An efficient, patient friendly method to detect retinal exudates based on binary operation is presented in this study. A novel Histogram equalization technique centered on intensity index is used for fundus image enhancement. Following the elimination of optic disc from the fundus image, morphological operation is performed to detect the exudate pixels. Finally, classification of hard exudates using a trained Support Vector Machine (SVM) classifier is implemented and evaluated using five different performance parameters. The results are assuring and recommends that the proposed method can be utilized as an analytic aid to ophthalmologist for early detection of retinopathy symptoms.

Index Terms*: *Diabetic Retinopathy, Image Enhancement, Exudate detection, Support Vector Machine classification.

I. INTRODUCTION

Retinal exudates which is one of the symptom of Diabetic retinopathy(DR) can be seen as yellow flecks in RGB fundus images. These are leakage of lipids from the damaged capillaries of eyes as shown in Figure 1. An early detection of retinal exudate can curb the extent of damage caused by this serious leakage of lipids which eventually may lead to vision loss. Non-invasive studies about exudate detection focusses on how accurately exudates can be detected from fundus images by machine learning. Images captured using a fundus camera can contain noise and vignette effects. These are to be filtered out before further processing of clinical images. From literature, it is studied that image enhancement is the area that requires more focus while dealing with fundus images having low intensity. The work presented in [1]detects retinal exudates based on spider monkey optimization using an SMO-GBM classifier. Also, the image enhancement was done using contourlet transform. Top-k loss method of classification is proposed in [2] instead of class balance cross entropy(CBCE) for exudate segmentation in order to reduce misclassification. The study in [3] suggest

Figure 1

that convolutional neural network (CNN) can be used as a deep learning technique,for exudate detection, but the performance is poor when compared with Residual Network and Discriminative Restricted Boltzmann machines. The colour space used in our work is HSI instead of RGB, which gives more attenuation to noise. This method is reiterated by the work suggested by Khojastey et.al [4] for exudate detection. Holistic texture features of fundus images were extracted and trained to four different classifiers in the study [5] conducted on a public database. Classification of hard exudates from soft exudate using fuzzy logic was the area of interest in [6]. Segmentation of exudates using dynamic decision thresholding was the focus of study in [7]. Their results were validated using lesion and image based evaluation criteria. Circular Hough transform and CNN based detection of exudates was suggested in [8]. A reduced pre-processing strategy for exudate based macular edema recognition using deep residual network was put forward in [9]. Multilayer perceptron based supervised learning is studied in [10] to identify exudate pixels. Further segmentation was done using unsupervised learning with the help of iterative graph cut (GC). The entire image is segmented into a series of super pixels in [11] which are considered as candidate pixels.

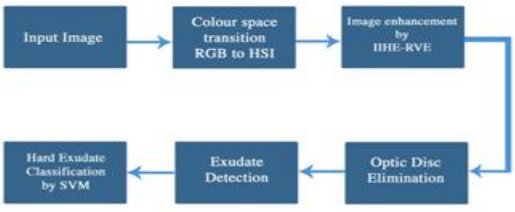

Figure 2

Also each candidate is characterized by multi-channel intensity features and contextual features. The study [12] using a neighborhood estimator presents vessel detection and segmentation by in-painting exudates with the help of this estimator. A voxel classification based approach using a layer dependent stratified sampling strategy on OCT image was introduced in [13].

Manuscript published on 30 June 2019.
***** Correspondence Author (s)
Arun Pradeep*, Department of Electronics and Communication Engineering, Noorul Islam University, Kanyakumari, Tamil Nadu, India.
X Felix Joseph, Department of Electrical and Electronics Engineering, NICHE & Bulehora University, Ethiopia.

Grayscale morphology based segmentation of exudates was presented in [14] where the candidate pixels' shape was determined with the help of Markovian segmentation model. A partial least squares (PLS) based classification to perform exudate detection is presented in [15]. A high level entity called splat is used to identify retinal hemorrhages in [16] where pixels sharing similar properties are grouped together to form non-overlapping splats and the features are extracted and classified using supervised learning. The research study presented in this paper is a modification of our existing algorithm presented in [17].The method associates both the principles of mathematical morphology operation for detection of exudates and classification and extraction of exudates using a trained classifier. Before the mathematical binary operation, Initial pre-processing is done to enhance the fundus image where an algorithm called Intensity Index based Histogram Equalization Technique for retinal vessel enhancement (IIHE-RVE) is proposed. The algorithm of the total work is depicted in Figure 2.

II. METHODOLOGY

The improved pre-processing step involves colour plane transition of the original fundus image from RGB to HSI. This is done since optic disc and exudates share similar intensity characteristics. It also reduces imperfections produced due to texture and noise in the image [18]. The noise in the intensity band is removed by applying median filter along the intensity band of the entire image. In order to enhance the contrast of the noise removed image the new method, Intensity Index based Histogram Equalization Technique for retinal vessel enhancement (IIHE-RVE) is performed. This method is different from existing Contrast limited adaptive histogram equalization(CLAHE) methods or Gaussian function based methods as it involves the estimation of under radiance of the image. In the next step, the optic disc is removed by assuming that the optic disc exists as the largest component with circular shape in the fundus image. In the second and final process, the exudates are classified as soft exudates and hard exudates using a support vector machine classifier. The data set is validated using clinical images and images from publically available database.

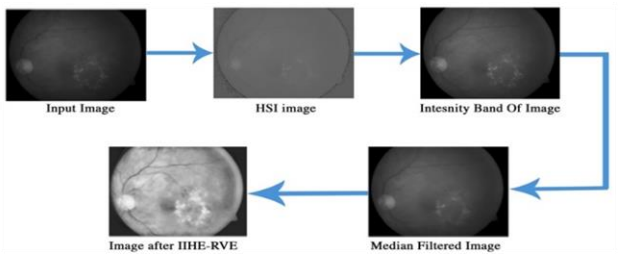

Figure 3

A. *Image Enhancement*

Figure 3 shows the pre-processing steps performed in our work. After colour plane transition from RGB to HSI and application of median filter, the enhancement of the fundus image is performed by the new proposed technique for histogram equalization.

Utilizing a tunable parameter ξ, histograms are separated into sub-histograms by calculating the split value using the following set of equations 1 and 2

$$\alpha_c(i) = \frac{\phi(i)}{\varepsilon} \; for \; 0 \le i \le I-1 \qquad (1)$$

$$\Gamma(k) = \sum_{i=0}^{k} \alpha_c(i) \; for \; 0 \le k \le I-1 \qquad (2)$$

Where, ϕ denotes, histogram of the image, i represents intensity value, ε represents the number of pixels in the whole image and I signifies the total intensity levels in numbers. The parameters Γ and α_c gives accumulated normalized histogram count and normalized histogram count respectively for the given image. The controlling parameter Γ_p is found by the equation 3.

$$\sum_{j=0}^{\Gamma_p} \Gamma(j) \approx \xi \; for \; any \; 0.1 \le \xi \le 0.9 \qquad (3)$$

The split value S_v is found from the equation 4

$$S_v = (I-1) - \Gamma_p - 1 \qquad (4)$$

The level of enhancement is inversely proportional to the value of tunable parameter ξ. Also when ξ increases the value of Γ_p also increases. For a particular low value of ξ, we can obtain a first sub histogram and for another high value of ξ we can obtain a second sub histogram. The first and second sub histograms are equalized distinctly. Due to the extendedness of these histograms, the range of pixels having lower intensity can be mapped to a range of higher intensity. Whereas, in the second sub histogram, the range is less and contains only larger intensity range pixels. Due to this small range, the larger intensity pixels are saved from over enhancement.

B. *Intensity Index based Histogram Equalization Technique for retinal vessel enhancement (IIHE-RVE)*

In this algorithm, after obtaining the two histograms they are integrated repeatedly based on the difference between intensity parameters determined from the iteratively enhanced image. The integration is performed until absolute difference between the iterative intensity values, ω_1 and ω_2 (from equation (5)) for the given image and the equalized image is less than the threshold error, e. The value of e is arbitrarily chosen as 0.002.

Algorithm for IIHE-RVE

1. Compute histogram ϕ for image f.
2. Compute intensity values for input image from eq. (5) for I = 256.

$$\omega_1 = \frac{\sum_{i=0}^{I-1} \phi(i).i}{I.\sum_{i=0}^{I-1} \phi(i)} \qquad (5)$$

3. Calculate split value S_v from eq. (4).
4. Separate the histograms into two sub histograms ϕ_l and ϕ_u from radiance range 0 to S_v and $S_{v+1}$to $I-1$ respectively.
5. Equalize histograms ϕ_l and ϕ_u in the respective intensity range.
6. Reiterate step 2 to find intensity value ω_2 of equalized image.
7. Perform steps 1-7 until $|\omega_1 - \omega_2| < e$
8. Integrate ϕ_l and ϕ_u to re-establish histogram ϕ.

Published By:
Blue Eyes Intelligence Engineering
& Sciences Publication (BEIESP)

C. *Optic Disc Elimination*

The optic disc shares similar intensity values of that of exudates. The binary operations such as opening, closing and erosion can be used to detect the optic disc. Initially, closing operation is applied in order to get the shape of the disc from the input Image I. The closing operation is followed by threshold method to obtain a binary image. The output of this threshold is image Ω that includes various connected regions such as C_i and it can be characterized as:

$$\Omega = \bigcup_{k \in m} C_k, C_i \bigcap C_j = 0, \forall\, i,j \in m, \qquad i \neq j \tag{6}$$

Where, m varies from $1\ to\ k, k$ is the total number of components connected in the image. Compared with the background, the components have additional pixels and has a disc shape structure which belongs to C_i where in which the optic disc is also included. Thus effective separation of optic disc from other structures of C_i is established. Now, R_i forms the biggest component that is included in C_i. The conciseness of R_i can be measured using the formula as:

$$C(R_i) = 4\pi \frac{A(R_i)}{P^2(R_i)} \tag{7}$$

Where, $A(R_i)$ signifies the number of pixels in the i^{th} region and $P(R_i)$ represents the pixels out of the region (R_i). The threshold method to get the binary image is deduced from P-tile method [19] and Nilback's method[20][21]. The weight factor chosen is 1.3 based on previous conclusions in our method [17]. In order to isolate the optic disc from the entire

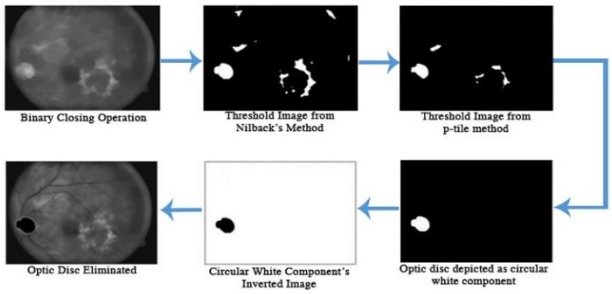

Figure 4

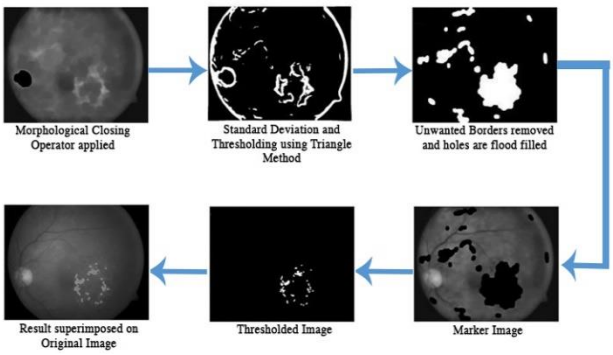

Figure 5

image, Circular Hough Transformation method is used [22]. The OD elimination is depicted in Figure 4.

D. *Detection of exudates*

After optic disc elimination, exudate pixels are identified. Using binary closing operation with a structuring element of flat disc shape of 16-pixel radius, the exudates pixels are directly identified. Following the threshold operation, a closing operation is applied. The contrast component for this operation is same as for the blood vessels. So, the standard deviation of the image has is calculated using the equation.

$$I_3(x) = \frac{1}{N-1} \sum_{i \in W(x)} \left(I_2(i) - \overline{I_3(x)}\right)^2 \tag{8}$$

Where, *W(x)* represents the pixels available in the sub-window, *N* represents the total number of pixels in *W(x)* and $\overline{I_3(x)}$ represents the mean value of the image $I_3(x)$ and I_3 represents the local contrast image. Using Triangle thresholding method [23], the bright regions can be precisely detected and the components can be differentiated. Followed by detection of these bright regions, unwanted regions on the image are removed using dilation operation. The dilation method is followed by a flood filling operation performed on the holes so as to reconstruct the image. The final step involved in detection of exudates is to take the difference between the output image and threshold image, i.e. intensity based image. The result of difference is superimposed in the real RGB image for feature extraction from the exudate pixels. The exudate detection performed is depicted in Figure 5.

E. *Hard Exudate Classification*

The final operation, which is the hard exudate classification, comprises of a feature set which were used by retinal experts to visually distinguish hard exudates. These feature sets are used as inputs of Support Vector Machine (SVM) Classifier. The feature set is shown in Table I. Compared with features published in algorithms [24][25][26], the eight features mentioned in Table I were measured necessary to decrease execution time without compromising the accuracy for hard exudate classification. The features extracted and mentioned in Table I are now fed to a trained SVM classifier where the output is a binary matrix that depicts the classification results. SVM is applied over Radial basis function (RBF) kernel.

Table I

Feature Number	Feature Name	Description
f1	Mean Channel Green Intensity	Mean filter of size 3 x 3 was applied to the green channel image to indicate gray scale intensity for every pixel.
f2	Gray Intensity	Gray scale value for each pixel.
f3, f4, f5	Mean hue, mean saturation and mean intensity in HSI colour model.	Mean filter of size 3 x 3 respectively, applied to the three channel image I_h, I_s, I_i. Exudates occur as bright lesions on the surface of retina hence the information about saturation and brightness (f4 and f5) is important.
f6		
f7	Energy	Summation of pixel value intensity squares.
f8	Standard Deviation Mean Gradient Magnitude	Morphological opening operation was applied to the image to preserve foreground regions that shares similar characteristics to the structuring element. Magnitude of directional change in intensity of edge pixels.

Published By:
Blue Eyes Intelligence Engineering
& Sciences Publication (BEIESP)

Cross validation and training was done using ground truth images that were manually selected by a retinal expert obtained from Bhejan Singh Eye hospital. 72 images selected from ground truth were taken as training samples. The regions in the selected images were divided as exudate and non-exudate regions. A 10-fold cross validation was performed to evaluate the efficiency of the SVM classifier. Selected images from the database DIARETDB1 was arbitrarily split into 10 mutually exclusive exudate connected component subsets (i.e., 10 folds) $B_1, B_2, B_3 \ldots\ldots B_{10}$ having equal size. The SVM classifier was trained on 67 images from the selected ground truth. The remaining 5 images were tested and the binary matrix is obtained as the output. The operation was repeated 10-fold. Each pixels reverted a feature vector p_i containing the eight feature sets as :

$$a_i = (f1, f2, f3, \ldots\ldots f10) \qquad (9)$$

Another entity q_j forms the category flag and is denoted as

$$b_j = \begin{cases} -1, & a_i \in A \\ +1, & a_i \in B \end{cases} \qquad (10)$$

where $\subset \{1,2 \ldots\ldots W\}$, W represents the sample vector set dimension. A and B represents hard exudate and non-hard exudate regions respectively.

The training sample set (a_i, b_j) was fed as input to train the SVM classifier. In this work W = 4200 i.e. 4200 from the 67 training images were selected by an expert.

F. *Evaluation on DIARETDB1 database*

In this research work, a hybrid cross-validation method is used. The database exudate subset $\{B_1, B_2, B_3 \ldots\ldots B_N\}$ and the ground truth exudate subset $\{T_1, T_2, T_3 \ldots\ldots T_M\}$ we can write as follows.

A pixel is considered true positive(TP) if

$$\{B \cap T\} \cup \left\{B_i \middle| \frac{|B_i \cap T|}{|B_i|} > \sigma\right\} \cup \left\{T_j \middle| \frac{|T_j \cap B|}{|G_j|} > \sigma\right\} \qquad (11)$$

The value of σ ranges from 0 to 1 and it is being arbitrarily chosen as 0.2 in this work.

Likewise, a pixel is considered as a false positive (FP) if

$$\{B_i | B_i \cap T = \emptyset\} \cup \left\{B_i \cap \bar{T} \middle| \frac{|B_i \cap T|}{|B_i|} \leq \sigma\right\} \qquad (12)$$

And the pixel is a false negative (FN) if

$$\{T_j | T_j \cap B = \emptyset\} \cup \left\{T_j \cap \bar{B} \middle| \frac{|T_j \cap B|}{|T_j|} \leq \sigma\right\} \qquad (13)$$

Now the pixels that remains are considered as true negatives (TN).

III. Results and Discussion

The fundus images were acquired from two sources. Clinical images were obtained from Dr. Bhejan Singh's eye hospital. The clinical image was captured using a "Remidio Non-Mydriatic Fundus On Phone (FOP-NM10)" [27] Camera with FOV 40°, working distance of 33mm and an ISO range from ISO 100 to 400. The images used for validation was acquired from the publically available database DIARETDB1(http://www.it.lut.fi/project/imageret/diaretdb1/index.html). Since there is an asymmetry between the classes of TP, FN and FP when compared with TN, by computing just the Receiver operator characteristic AUC (Area under curve) is not appropriate. So 5 different evaluation parameters are taken into consideration. They are:

$$Accuracy = \frac{TN + TP}{TP + FP + TN + FN}$$

$$Sensitivity = \frac{TP}{TP + FN}$$

$$Specificity = \frac{TN}{TN + FP} \qquad (14)$$

$$Positive\ prediction\ value\ (PPV) = \frac{TP}{TP + FP}$$

$$F\ Score = 2\ X\ \frac{Sensitivity\ X\ PPV}{Sensitivity + PPV}$$

Published By:
Blue Eyes Intelligence Engineering
& Sciences Publication (BEIESP)

Table II

	TP	FN	FN	TN	Accuracy	Sensitivity	Specificity	PPV	F-Score
Image 1	349	0	0	431651	100.00%	100.00%	100.00%	100.00%	100.00%
Image 2	372	35	106	431487	99.97%	77.82%	99.99%	91.40%	84.07%
Image 3	6835	0	700	419183	99.84%	90.71%	100.00%	100.00%	95.13%
Image 4	54	0	0	431946	100.00%	100.00%	100.00%	100.00%	100.00%
Image 5	321	0	49	431630	99.99%	86.76%	100.00%	100.00%	92.91%
Image 6	1488	0	600	429122	99.86%	71.26%	100.00%	100.00%	83.22%
Image 7	409	68	103	431420	99.96%	79.88%	99.98%	85.74%	82.71%
Image 8	964	286	0	430947	99.93%	100.00%	99.93%	77.12%	87.08%
Image 9	6543	68	300	422555	99.91%	95.62%	99.98%	98.97%	97.26%
Image 10	811	278	137	430774	99.90%	85.55%	99.94%	74.47%	79.63%
Image 11	1166	250	49	430535	99.93%	95.97%	99.94%	82.34%	88.64%
Image 12	3522	0	700	427474	99.84%	83.42%	100.00%	100.00%	90.96%
Image 13	818	254	0	430259	99.94%	100.00%	99.94%	76.31%	86.56%
Image 14	435	149	88	431328	99.95%	83.17%	99.97%	74.49%	78.59%
Image 15	1536	1275	505	428684	99.59%	75.26%	99.70%	54.64%	63.31%
Image 16	623	0	200	431002	99.95%	75.70%	100.00%	100.00%	86.17%
Image 17	3421	0	200	427567	99.95%	94.48%	100.00%	100.00%	97.16%
Image 18	4090	0	452	427468	99.90%	90.05%	100.00%	100.00%	94.76%
Image 19	233	0	67	431731	99.98%	77.67%	100.00%	100.00%	87.43%
Image 20	785	52	110	431053	99.96%	87.71%	99.99%	93.79%	90.65%
Image 21	327	0	110	431563	99.97%	74.83%	100.00%	100.00%	85.60%
Image 22	1053	0	0	430947	100.00%	100.00%	100.00%	100.00%	100.00%
Image 23	188	223	70	431441	99.93%	72.87%	99.95%	45.74%	56.20%
Image 24	2213	45	100	429216	99.97%	95.68%	99.99%	98.01%	96.83%
Image 25	964	286	0	430750	99.93%	100.00%	99.93%	77.12%	87.08%
Image 26	521	0	29	431650	99.99%	94.73%	100.00%	100.00%	97.29%
Image 27	848	0	300	429132	99.93%	73.87%	100.00%	100.00%	84.97%
Image 28	904	82	223	431480	99.93%	80.21%	99.98%	91.68%	85.57%
Image 29	842	254	18	430927	99.94%	97.91%	99.94%	76.82%	86.09%
Image 30	4543	68	200	422565	99.94%	95.78%	99.98%	98.53%	97.13%
Avg. Value					99.92%	87.90%	99.97%	89.91%	88.10%

Table III

Methodology	Sensitivity %	Specificity %	Accuracy %
Chen et. al [29]	83	75	79
Travieso et. al [30]	91.67	92.68	92.13
Barman et. al [31]	92.42	81.25	87.72
Proposed method	87.9	99.97	99.92
A Hajdu et. al [26]	92	68	82
R Sinha et. al [25]	96.54	93.15	N.A.
Pourreza et. al [28]	86.01	99.93	N.A.

The precision or PPV combined with TP and FP denotes the ratio of detected exudate pixels with the number of pixels labelled by the expert. In 30 images that were validated, an average sensitivity, specificity and accuracy of 87% ,99% and 99% respectively were obtained. Also the precision and f-score was comparatively higher than other algorithms in literature[28][29] which is 89.91% and 88.10 % respectively. Table III gives a comparison with other published algorithms and it indicates that the specificity and accuracy of our method is truly higher than others.

Table IV gives a comparison of the improved method of image enhancement that is IIHE-RVE with our previous method-Contrast limited adaptive histogram equalization (CLAHE) which shows a reasonable increase in the value of specificity, PPV and F-score.

Table IV

Features	Methodology	
	CLAHE [17]	IIHE-RVE
Sensitivity	99.81	99.92
Specificity	80.06	87.90
Accuracy	99.96	99.97
PPV	88.03	89.91
F-Score	81.90	88.10

IV. CONCLUSION

The proposed work is a novel technique to detect exudates using morphological operation. The new enhancement method IIHE-RVE was used to increase the sensitivity of our existing algorithm that originally involved enhancement using CLAHE. A considerable increase in specificity indicates that the algorithm is more accurate while considering low intensity images. Using the same feature set to the classifier, the score of evaluation parameters could be increased by changing the enhancement technique. Further studies can be implicated to increase the PPV and F-Score of this algorithm.

REFERENCES

1. R. D. Badgujar and P. J. Deore, "Hybrid Nature Inspired SMO-GBM Classifier for Exudate Classification on Fundus Retinal Images," *IRBM*, vol. 40, no. 2, pp. 69–77, Mar. 2019.
2. S. Guo, K. Wang, H. Kang, T. Liu, Y. Gao, and T. Li, "Bin loss for hard exudates segmentation in fundus images," *Neurocomputing*, Apr. 2019.
3. P. Khojasteh *et al.*, "Exudate detection in fundus images using deeply-learnable features," *Comput. Biol. Med.*, vol. 104, pp. 62–69, Jan. 2019.
4. P. Khojasteh, B. Aliahmad, and D. K. Kumar, "A novel color space of fundus images for automatic exudates detection," *Biomed. Signal Process. Control*, vol. 49, pp. 240–249, Mar. 2019.
5. L. B. Frazao, N. Theera-Umpon, and S. Auephanwiriyakul, "Diagnosis of diabetic retinopathy based on holistic texture and local retinal features," *Inf. Sci. (Ny).*, vol. 475, pp. 44–66, Feb. 2019.
6. R. S. Kumar, R. Karthikamani, and S. Vinodhini, "Mathematical Morphology for Recognition of Hard Exudates from Diabetic Retinopathy Images," *International Journal of Recent Technology and Engineering (IJRTE) Volume 7, Issue 4S*, 2018.
7. J. Kaur and D. Mittal, "A generalized method for the segmentation of exudates from pathological retinal fundus images," *Biocybern. Biomed. Eng.*, vol. 38, no. 1, pp. 27–53, Jan. 2018.
8. K. Adem, "Exudate detection for diabetic retinopathy with circular Hough transformation and convolutional neural networks," *Expert Syst. Appl.*, vol. 114, pp. 289–295, Dec. 2018.
9. J. Mo, L. Zhang, and Y. Feng, "Exudate-based diabetic macular edema recognition in retinal images using cascaded deep residual networks," *Neurocomputing*, vol. 290, pp. 161–171, May 2018.
10. W. Kusakunniran, Q. Wu, P. Ritthipravat, and J. Zhang, "Hard exudates segmentation based on learned initial seeds and iterative graph cut," *Comput. Methods Programs Biomed.*, vol. 158, pp. 173–183, May 2018.
11. W. Zhou, C. Wu, Y. Yi, and W. Du, "Automatic Detection of Exudates in Digital Color Fundus Images Using Superpixel Multi-Feature Classification," *IEEE Access*, vol. 5, pp. 17077–17088, 2017.
12. R. Annunziata, A. Garzelli, L. Ballerini, A. Mecocci, and E. Trucco, "Leveraging Multiscale Hessian-Based Enhancement With a Novel Exudate Inpainting Technique for Retinal Vessel Segmentation," *IEEE J. Biomed. Heal. Informatics*, vol. 20, no. 4, pp. 1129–1138, Jul. 2016.
13. X. Xu, K. Lee, L. Zhang, M. Sonka, and M. D. Abramoff, "Stratified Sampling Voxel Classification for Segmentation of Intraretinal and Subretinal Fluid in Longitudinal Clinical OCT Data," *IEEE Trans. Med. Imaging*, vol. 34, no. 7, pp. 1616–1623, Jul. 2015.
14. B. Harangi and A. Hajdu, "Detection of exudates in fundus images using a Markovian segmentation model," in *2014 36th Annual International Conference of the IEEE Engineering in Medicine and Biology Society*, 2014, vol. 2014, pp. 130–133.
15. C. Agurto *et al.*, "A Multiscale Optimization Approach to Detect Exudates in the Macula," *IEEE J. Biomed. Heal. Informatics*, vol. 18, no. 4, pp. 1328–1336, Jul. 2014.
16. K. A. Sreeja and S. S. Kumar, "Comparison of Classifier Strength for Detection of Retinal Hemorrhages," *Int. J. Innov. Technol. Explor. Eng.(IJITEE.org)*, vol. 8, no. 6S3, pp. 688–693, 2019.
17. P. Arun and J. X. Felix, "Retinal exudate detection using binary operation and hard exudate classification using support vector machine," *IJITEE.org*, vol. 8, no. 9, 2019.
18. S. Arpit and M. Singh, "Speckle Noise Removal and Edge Detection Using Mathematical Morphology," *International Journal of Soft Computing and Engineering* Volume 1, Issue 5, Nov. 2011.
19. M. Taghizadeh and M. R. Mahzoun, "Bidirectional Image Thresholding Algorithm Using Combined Edge Detection And P-tile Algorithms," *J. Math. Comput. Sci.*, vol. 02, no. 02, pp. 255–261, Feb. 2011.
20. M. S. H. Naveed Bin Rais, "Adaptive thresholding technique for document image analysis," in *8th International Multitopic Conference, 2004. Proceedings of INMIC 2004.*, pp. 61–66.
21. G. Leedham, Chen Yan, K. Takru, Joie Hadi Nata Tan, and Li Mian, "Comparison of some thresholding algorithms for text/background segmentation in difficult document images," in *Seventh International Conference on Document Analysis and Recognition, 2003. Proceedings.*, vol. 1, pp. 859–864.
22. S. Long, X. Huang, Z. Chen, S. Pardhan, and D. Zheng, "Automatic Detection of Hard Exudates in Color Retinal Images Using Dynamic Threshold and SVM Classification: Algorithm Development and Evaluation," *Biomed Res. Int.*, vol. 2019, pp. 1–13, Jan. 2019.
23. M. Baisantry, D. S. Negi, and O. P. Manocha, "Change vector analysis using enhanced PCA and inverse triangular function-based thresholding," *Def. Sci. J.*, 2012.
24. M. U. Akram, A. Tariq, S. A. Khan, and M. Y. Javed, "Automated detection of exudates and macula for grading of diabetic macular edema," *Comput. Methods Programs Biomed.*, vol. 114, no. 2, pp. 141–152, Apr. 2014.
25. M. Haloi, S. Dandapat, and R. Sinha, "A Gaussian Scale Space Approach For Exudates Detection, Classification And Severity Prediction," ICIP, May 2015.
26. B. Harangi and A. Hajdu, "Automatic exudate detection by fusing multiple active contours and regionwise classification," *Comput. Biol. Med.*, vol. 54, pp. 156–171, Nov. 2014.
27. "Remidio Non-Mydriatic Fundus On Phone (FOP-NM10)."
28. E. Imani and H.-R. Pourreza, "A novel method for retinal exudate segmentation using signal separation algorithm," *Comput. Methods Programs Biomed.*, vol. 133, pp. 195–205, Sep. 2016.
29. Q. Liu, J. Chen, W. Ke, K. Yue, Z. Chen, and G. Zhao, "A location-to-segmentation strategy for automatic exudate segmentation in colour retinal fundus images," *Comput. Med. Imaging Graph.*, vol. 55, pp. 78–86, Jan. 2017.
30. R. S. Rekhi, A. Issac, M. K. Dutta, and C. M. Travieso, "Automated classification of exudates from digital fundus images," in *2017 International Conference and Workshop on Bioinspired Intelligence (IWOBI)*, 2017, pp. 1–6.
31. M. M. Fraz, W. Jahangir, S. Zahid, M. M. Hamayun, and S. A. Barman, "Multiscale segmentation of exudates in retinal images using contextual cues and ensemble classification," *Biomed. Signal Process. Control*, vol. 35, pp. 50–62, May 2017.

Authors Profile

Arun Pradeep is a Research Scholar at Noorul Islam University, Tamil Nadu. He received his B.Tech. in Electronics and Communication Engg. in 2009 and M.tech. in Embedded Systems in 2012. He was an Assistant professor in Electronics and Communication Engineering. at Axis College of Engineering, Thrissur, Kerala during the period 2012 to 2018. His research interest field is Medical Image processing.

X. Felix Joseph is an Assistant Professor at Bulehora University, Ethiopia. Dr. Felix Joseph has more than 14 years of experience in the teaching field in the area of Electrical and Electronics, He has attended more than 60 short term training programs including two weeks STTP, one-week seminar, one day workshops, and two weeks training programs. Currently he is guiding seven research scholars and published more than 10 papers in international journals and conferences. His areas of interests are soft computing applications in digital signal processing, digital image processing and power electronics. His favorite subject is neural network, which is one of the tool used in soft computing techniques.